The impact of the differential arm length servo on photon calibrator comparisons

Paluku Makelele

Kenyon College
LIGO Hanford Observatory

Mentors: Richard Savage and Dripta Bhattacharjee

Abstract. The detectors of the Laser Interferometer Gravitational-Wave Observatory (LIGO) are enhanced Michelson interferometers with four-km-long arms and 40 kg suspended mirrors. They detect differential arm length (DARM) fluctuations as small as 10^{-19} m. A DARM servo maintains the interference condition and the servo error point and control signals are used to compute relative length changes induced by gravitational waves. To provide accurate absolute calibration, a Photon Calibrator (Pcal) system has been implemented at the end of each interferometer arm. By leveraging the insensitivity of the interferometer to which arm length is changing, calibration uncertainty can be reduced by comparing Pcal fiducial displacements at two closely separated frequencies using a signal from the DARM servo. This comparison has been calculated continuously using the reconstructed *external* length variation signal by the LIGO group at Kenyon College since the beginning of the ongoing O4 observing run. Drifts as large as 0.2 % were observed in the LIGO Hanford Observatory (LHO) data over a year-long interval. To investigate the potential impact of changes in the DARM servo response at the two Pcal excitation frequencies, the Kenyon group also calculated the comparison using the DARM loop error signal. The ratio of the comparison calculated using the two methods yields the suppressed DARM loop sensing ratio. Data from May 2023 that includes the first six days of the ongoing O4 observing run reveal that the relative changes in the ratio of the response of the DARM servo at the two Pcal excitation frequencies were smaller than 0.0022 %. This may indicate that DARM servo response variations are not a significant contributor to the 0.2 % drifts observed in the Pcal calibration comparison factor. Efforts to extend this investigation to the rest of the O4 run data are ongoing.
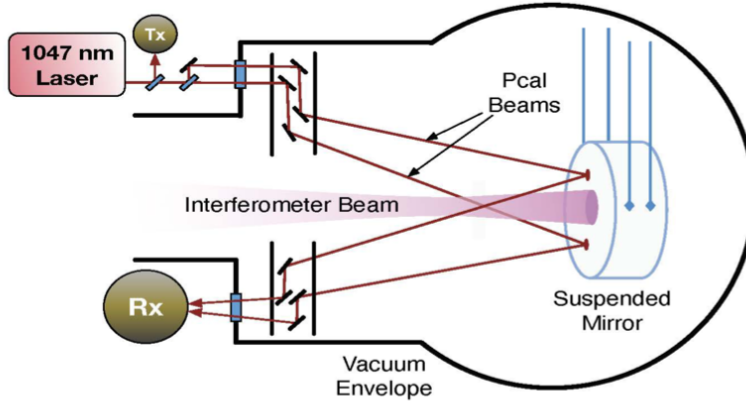
Figure 1: Schematic diagram of a photon calibrator system from [1]. A small fraction of the power-modulated laser is sampled by a power sensor (Tx) inside a transmitter module. This allows us to estimate the optical losses inside the vacuum chamber when the power of the beam reflected off the surface of the suspended mirror is measured by the Rx sensor in the receiver module after exiting the vacuum chamber. The suspended mirror experiences displacements proportional to the incident laser power.

Introduction

The Laser Interferometer Gravitational-Wave Observatory (LIGO) detects gravitational waves by measuring their induced length variations, often smaller than 10^{-19} m. It uses enhanced Michelson Interferometers with 4 km-long perpendicular optical cavities referred to as the X-arm and the Y-arm. Precise and accurate calibration of these detectors is needed to extract the encoded astrophysical information and differentiate gravitational wave signals from noise of terrestrial origin. Photon Calibrator (Pcal) systems are the primary calibration reference for LIGO observatories. Figure 1 shows a schematic diagram of a Pcal system installed in a vacuum chamber at the end stations of the interferometer, where the end test masses (ETMs)reside. They include a 1047 nm power-modulated laser, power sensors consisting of unbiased InGaAs photodetectors, relay mirrors, and beam splitters. The laser output is divided into two beams that, after being directed into a vacuum chamber, reflect from the surface of a suspended ETM. The reflected power exiting the vacuum chamber is measured by a Pcal power sensor, referred to as the Rx sensor. The photon radiation pressure from the Pcal beams causes length variations with magnitudes that are directly proportional to the modulated laser power reflecting from the mirror. Thus, accurate and precise measurement of the reflected beam power is a key step in generating accurately calibrated length variations.

Motivation

Each LIGO interferometer has two Pcal systems, one at the end of each arm. They are referred to as PcalX and PcalY. By design, LIGO interferometers respond equally to length variations of either arm. This feature enables the assessment of the relative calibration between the two Pcal systems using the interferometer output signals as well as the monitoring of small variations in the relative Pcal system calibrations. The comparison is achieved by modulating each Pcal system at one of two closely separated frequencies (0.1 Hz separation). We calculate a ratio of the amplitudes of PcalX-induced ETM motion and PcalY-induced ETM motion at the two frequencies. Each modulation amplitude is normalized to the amplitude of the peak in an interferometer signal that senses the motion induced by the respective Pcal system. This ratio is referred to as the Pcal X/Y comparison factor, χ_{XY}, and is mathematically denoted as:

$$\chi_{XY} = \frac{x(\omega_X)|_{PcalX}/DARM(\omega_X)}{x(\omega_Y)|_{PcalY}/DARM(\omega_Y)} \tag{1}$$

$x(\omega)|_{Pcal}$ is the amplitude of Pcal-induced displacement on the ETM by a respective Pcal system, indicated by the subscript, and $DARM(\omega)$ is the amplitude of the Pcal-induced peak in the DARM signal. Both Pcal systems are calibrated by the same procedures. Therefore, we expect this ratio to be unity. However, due to various statistical and potential systematic errors [1], it slightly deviates from one.
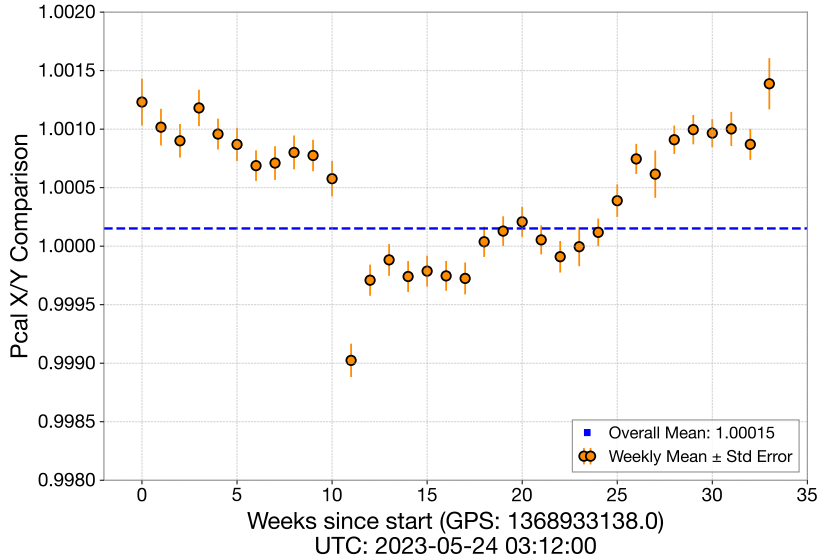

Figure 2: A 35-week time series plot of the variation of the Pcal comparison factor that begins from the start of the fourth observing run, May 24th, 2023. Each data point is the weekly mean of the χ_{XY} factor, with error bars given by the standard error multiplied by a by a factor of two to increase visibility.

3

Figure 2 shows that the value of χ_{XY} slowly drifts by about 0.2 % in during the first 20 weeks after the beginning of the O4 observing run. It begins to drift back, returning close to its initial value by week 35. The cause of this variation is not known, though it appears to be related to the outside average temperature. Potential changes in the DARM signal response to length variations over the 0.1 Hz separation between the two Pcal excitations would change the calculated value of χ_{XY}. The purpose of this project is to investigate the response function ratio's [2] role in this variation.

The Differential Arm Length (DARM) servo

Gravitational waves induce arm length changes onto the interferometer beams. The DARM servo calibrates this induced length change and restores the masses to their initial position. Strain, h, is mathematically denoted by[3]:

$$h = \frac{\Delta L_{free}}{L} = \frac{\Delta L_X - \Delta L_Y}{L} \tag{2}$$

where L is average the length of each arm, ΔL_{free} is the difference between the respective arm length changes, ΔL_X, and ΔL_Y. To maintain optical resonance, ΔL_{free} is not directly measured, but computed using the DARM servo shown in Figure 3 below. These computations are done in the frequency domain.
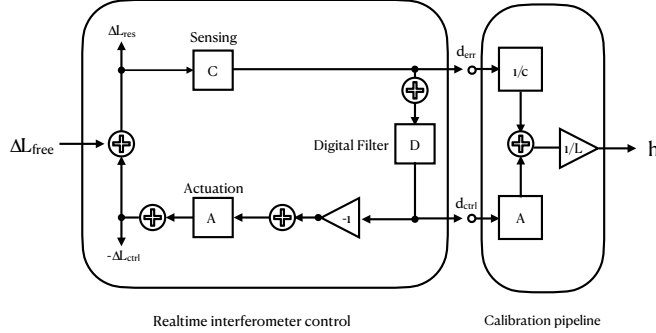

Figure 3: A schematic of the differential arm (DARM) length feedback control and calibrated strain data derivation loops. The sensing function C converts the residual DARM displacement, ΔL_{free}, to the digital error signal d_{err}. The digital filter, D, processes d_{err} and produces the digital control signal d_{ctrl}. The actuation function, A, converts the digital control signal to the control force allocated to the test masses that form the arm cavities, producing displacement $-\Delta L_{free}$ to suppress ΔL_{free}. The estimated DARM strain, h, is constructed on the right-hand side using the sensing and actuation models[3].

Calibrating the interferometer involves reconstructing the strain signal from the digital output of the interferometer photodetector signal. Mathematically this is represented as:

$$\Delta L_{free} = \Delta L_{res} + \Delta L_{ctrl} = \frac{d_{err}}{C} + d_{ctrl}A \tag{3}$$

The servo in Figure 3 shows that $d_{ctrl} = d_{err}D$. Therefore, ΔL_{free} is given by:

$$\Delta L_{free} = \frac{d_{err}}{C} + d_{err}DA = derr\left(\frac{1 + ADC}{C}\right) \tag{4}$$

with $\frac{1+ADC}{C} = R$, our response function, we can plug in this value of ΔL_{free} back into equation (1) to get a value of strain given by:

$$h = \frac{d_{err}R}{L} \tag{5}$$

This is one value strain. For real-time data analysis another value of strain, derived from mathematical models of the actuation and sensing functions, is computed using the calibration pipeline (Right of Figure 3). ΔL_{free}, in this model is the sum of d_{err}/C and $d_{ctrl}A$. The details of this computation are given in [4].

The photon calibrator comparison factor

The main purpose of χ_{XY}, given by equation 1, is to compare Pcal calibrations between the X-end and the Y-end. The interferometer is designed to detect differential arm length variation induced by strain. However, it only outputs the total magnitude of the variations as it is not designed to allocate arm length variation to a specific arm. The χ_{XY} ratio provides a means through which we can compare how precise the pcal systems are by monitoring their ratio. Two versions of the pcal comparison factor are calculated. One version is calculated using the low latency interferometer signal, referred to as strain signal, and the other is calculated using the high latency signal, referred to as the DARM_ERR signal. To computing these ratios, correction factors C_X and C_Y are implemented on $x(\omega)|_{Pcal}$ to correct for uncertainties in factors not common to both endstations. Mathematically this is denoted as: [2]

$$x(\omega_X)|_{PcalX} = PcalX(\omega_X)C_X \tag{6}$$

$$x(\omega_Y)|_{PcalY} = PcalY(\omega_Y)/C_Y \tag{7}$$

The pcal comparison factor is computed using the feedback loop (high latency signal) in Figure 3 using formalism in [2] as follows:

$$\chi_{XY} = \frac{PcalX(\omega_X)C_X}{PcalY(\omega_Y)/C_Y}\frac{D_{err}(\omega_X)/R(\omega_X)}{D_{err}(\omega_Y)/R(\omega_Y)} = \frac{PcalX(\omega_X)}{PcalY(\omega_Y)}\frac{D_{err}(\omega_Y)}{D_{err}(\omega_X)}C_XC_YR_{XY} \tag{8}$$

This is simplifies to $\chi_{XY} = CC_{Derr}C_XC_YR_{XY}$ where:

$$CC_{D_{err}} = \frac{PcalX(\omega_X)}{PcalY(\omega_Y)}\frac{D_{err}(\omega_Y)}{D_{err}(\omega_X)} \quad and \quad R_{XY} = \frac{R(\omega_X)}{R(\omega_Y)} \tag{9}$$

From equation 8 we can algebraically deduce:

$$CC_{D_{err}} = \frac{\chi_{XY}}{C_X C_Y} \frac{1}{R_{XY}} \tag{10}$$

Ideally $\chi_{XY} = C_X C_Y$. Hence, the $CC_{D_{err}}$ is equal to the inverse of the response function. Note that $CC_{D_{err}}$ is the ratio of all four signal lines, i.e, the two pcal beams and the two interferometer beams.

R_{XY} is ratio of the response function computed at each endstation. This is given by:

$$R_{XY} = \left[\frac{1+G}{C}\right]_{\omega=\omega_X} \left[\frac{1+G}{C}\right]^{-1}_{\omega=\omega_Y} \tag{11}$$

where G is the loop gain given by G = ADC. Abbreviations explained in Figure 3 caption. This function quantifies the interferometer's response to pcal-induced displacements at both end stations.

Without much detail in the algebra, which can be done with similar steps as in the formalism in [2], χ_{XY} computed using the low latency strain signal is given by:

$$\chi_{XY} = \frac{PcalX(\omega_X)}{PcalY(\omega_Y)} \frac{x(\omega_Y)|_{strain}}{x(\omega_X)|_{strain}} C_X C_Y = CC_{strain} C_X C_Y \tag{12}$$

where CC_{strain} is given by:

$$CC_{strain} = \frac{PcalX(\omega_X)}{PcalY(\omega_Y)} \frac{x(\omega_Y)|_{strain}}{x(\omega_X)|_{strain}} \tag{13}$$

Hence:

$$CC_{strain} = \frac{\chi_{XY}}{C_X C_Y} \tag{14}$$

The ratio of CC_{strain} and $CC_{D_{err}}$ yields a measure of the response function ratio as follows:

$$\frac{CC_{strain}}{CC_{D_{err}}} = \frac{\frac{\chi_{XY}}{C_X C_Y}}{\frac{\chi_{XY}}{C_X C_Y R_{XY}}} = \frac{\chi_{XY}}{C_X C_Y} \frac{C_X C_Y R_{XY}}{\chi_{XY}} = R_{XY} \tag{15}$$

The focus of this paper is the investigation of the response function ratio in order to observe how much it varies over time, and determine whether it is a factor in the variation observed by in the Pcal X/Y comparison in Figure 2.

Data collection

The Kenyon Line Monitoring (KLM) tool, which I designed using the framework of an existing line monitoring tool in the summer of 2023, processes real-time pcal-induced displacement data by taking using 480-second worth of data, and computes three 240-second Fourier Transforms, with a 50% overlap gives an average of the three data points every 60-sec to calculate a value of CC_{strain} every two minutes, as well as compute a running mean and median on the data. The KLM tool uses Kafka to stream this live data to the Grafana Pages[5]. That data is then stored in an InfluxDB database. This tool has been used since the start of the O4 observing run to store values of CC_{strain}, as it has varied over time. We are still populating InfluxDB with $CC_{D_{err}}$ values derived for the O4 run. We will use its stored data to compute the overall response function ratio, R_{XY}.

We have collected data from May 24 to June 1, 2023, and March 21 to March 26, 2024. These periods have 3504 and 2785 data points respectively. There have been efforts made by Professor Madeline Wade of Kenyon College, who possesses the technical expertise on the InfluxDB database system, to populate the database with more $CC_{D_{err}}$ data, but the Kafka server has been overpopulated with jobs that prevented us from getting $CC_{D_{err}}$ data for the full o4 run this summer. This was frustrating as the intention of this project is to analyze the response function ratio, R_{XY}, behavior in the 0.1 % variation we observed in Figure 2, and understand its role in causing that drift. We expected each data point of CC_{strain} and $CC_{D_{err}}$ to have a synchronized time axis. However, 12% of the data from May 2023 exhibit a time discrepancy. Specifically, these portions of the data are unsynchronized by a magnitude of 32 seconds. Table 1 shows the cadence difference for three instances in the time series. Note that this happens 454 times. We reached out to Professor Madeline Wade for insight into this problem, but we still could not find the root cause of this time discrepancy. There was no time discrepancy in the March 2024 data. All the data we used were from time segments when the interferometer was in a locked state, and actively observing for gravitational waves. While efforts are currently being made to find the cause of this time, we are still including this piece of data in our data sets.

GDS SIGNAL	DARM_ERR SIGNAL
96.0	64.0
64.0	96.0
96.0	64.0

Table 1: Three instances of time differences within the GPS and DARM_ERR time series in seconds

Data visualization

As explained by equation 15, we need to compute the ratio of $CC_{Strain}/CC_{D_{err}}$ to determine the response function ratio, R_{XY}. For our analysis, we extracted a time series from the influxDB database of CC_{strain} and $CC_{D_{err}}$ from May 24, 2023, to June 1, 2023, and March 21 to March 26, 2024. Figure 4 shows the subplots of the respective datasets. We are using the medians of the data sets
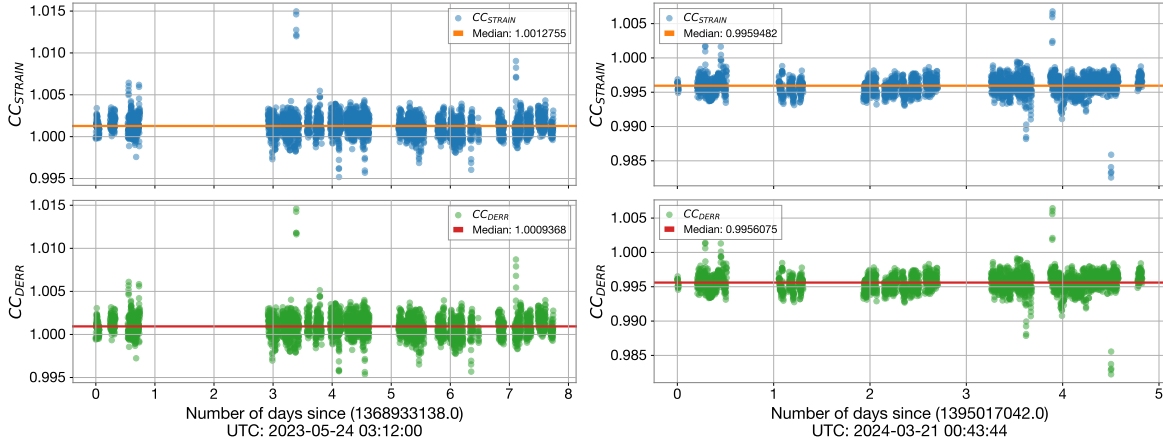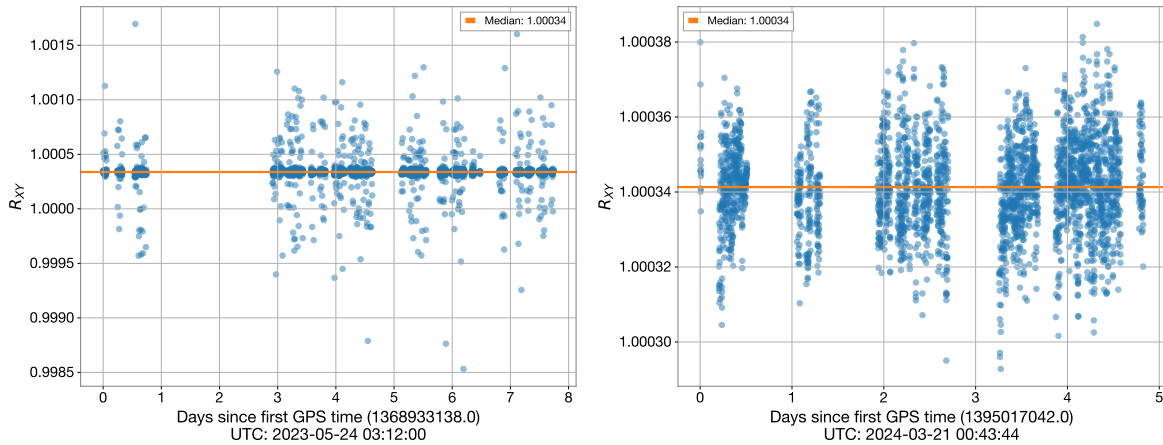
(a) May 24 to June 1, 2023   (b) March 21 to March 26, 2024

Figure 4: The corrected Pcal X/Y calibration comparison factor calculated via DARM loop error signal (*top*) and the calibrated strain signal (*bottom*) for May 24 to June 1, 2023, on the left and March 21 to March 26, 2024, on the right. Each data point is average of 240-second long FFTs calculated across 480-second data chunk with 50 % overlap. Only the observing segments during the respect periods were used to calculate the calibration comparison factor. The respective median of the two sets of data are noted in the legend.

Dividing the two datasets point for point $CC_{strain}/CC_{D_{err}}$ we get a value of R_{XY}, from mathematic models we expect most of our data points to be close to 1.00035 [2]. Figure 5 shows the values of R_{XY} as a scatterplot, and a histogram. These plots show that most of the R_{XY} values are within a tenth of a percentage from the median.

(a) May 24 to June 1, 2023   (b) March 21 to March 26, 2024

Figure 5: A ratio of the corrected Pcal X/Y calibration comparison factors calculated via DARM loop error signal (*top*) and the calibrated strain signal (*bottom*) for May 24 to June 1, 2023, and March 21 to March 26, 2024. This ratio is referred to as the response function ratio, R_{XY}.

Figure 5 shows that most of the data for May 2023 and March 2024 are within 0.001 %

of the median line of 1.00034, which is very close to our expected value of R_{XY}, 1.00035. However, The values in 5a show that the data there could be outliers. We expect our CC_{strain} and CC_{Derr} data to be completely random and follow a normal distribution. However, the physical process with which this data is obtained is susceptible to glitches that have the potential to cause outliers in our data. Below is a histogram of the raw data. We observe that outliers are affecting the distribution of the data.
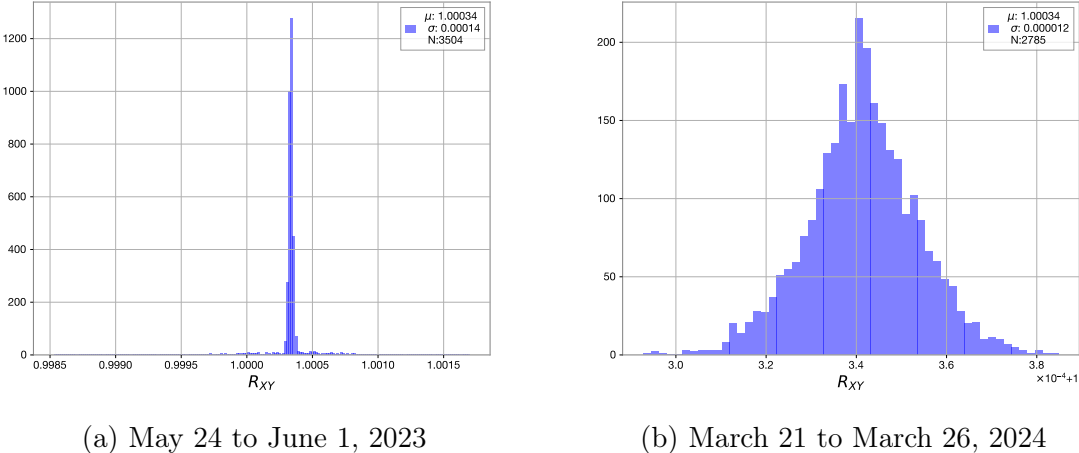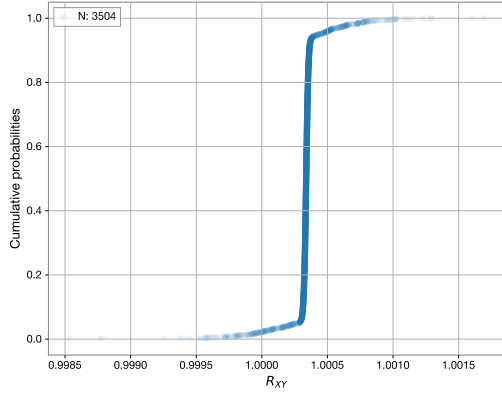

(a) May 24 to June 1, 2023

(b) March 21 to March 26, 2024

Figure 6: Histogram of data in Figure 5

Removing outliers using the Empirical Cumulative Distribution Function

Whilst the data points in our histograms form a symmetric shape we can see, especially in 6a that outliers have an influence on the overall shape of the data, preventing the bell-shaped curve of a normal (Gaussian) distribution [6]. Once these outliers are removed our data will follow a normal distribution. Hence, we calculated an empirical cumulative distribution function (ECDF) [7] because of its non-parametric nature. Afterward, we removed points until we had a distribution that mimics a cumulative distribution function Gaussian distribution. We then fitted a cumulative distribution function (CDF) of a Gaussian function to that data. This allows us to analyze the Gaussian proportion of R_{XY} data.
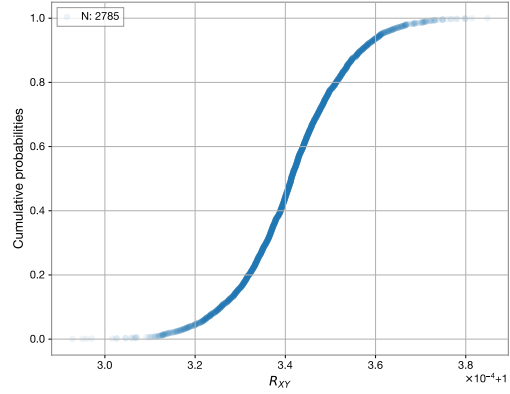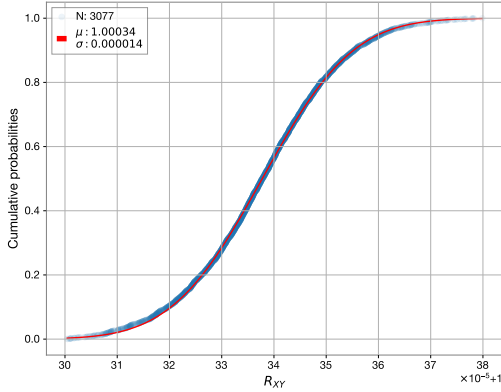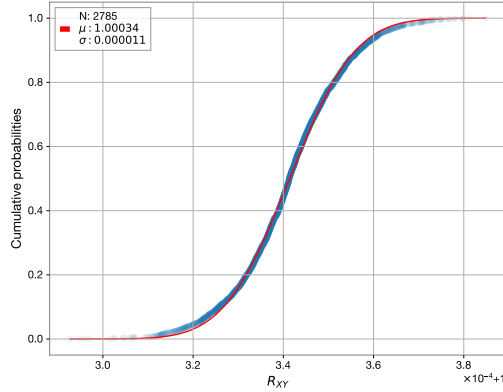
(a) May 24 to June 1, 2023   (b) March 21 to March 26, 2024

Figure 7: ECDF of data in Figure 5. The horizontal axis represents the values of R_{XY}, and the vertical axis represents the probability of data points that are less than or equal to the corresponding data value on the horizontal. The May 23 to June 1, 2023 data (*left*) looks almost like a step function which indicates that our data has outliers affecting its distribution. The March 21 to March 26, 2024 dataset (*right*) has a smooth S-shape. Similar to that of a CDF of a gaussian.

If our data is truly randomly distributed, the ECDF plot should have a smooth S-curve, resembling the function $f(x) = \frac{1}{1+e^{-x}}$. The March data set shows this distribution, telling us that all the data taken in March 2024 mimics a Gaussian distribution. On the other hand, the May 2023 data distribution mimics a step function indicating a few data points do not trend the same way as the overall dataset. With most of the points centered around the mean, 1.00034. To get the true distribution we removed data points up until we got a smooth S-curve for the May 2023 dataset. The distribution of both data sets looks to be approximately Gaussian in Figure 8, with the Mean of the datasets being 1.00034, with the standard deviations 1.4×10^{-5} and 1.1×10^{-5} for May 2023 and March 2024 respectively. Our expected value R_{XY} derived in [2] is 1.00035. The calculated and expected values agree at 0.001 % level. The small measured variations indicate that the response function ratio changes may not be significant in explaining the observed long-term drift (100 times larger) in the pcal calibration comparison.

(a) May 24 to June 1, 2023   (b) March 21 to March 26, 2024

Figure 8: ECDF of data in Figure 5 with a fitted CDF for a best fitting Gaussian function. The May 2023 dataset has had 11 % of its data removed. The horizontal axis represents the values of R_{XY}, and the vertical axis represents the probability of data points that are less than or equal to the corresponding data value on the horizontal.

The distribution of both data sets looks to be approximately Gaussian in Figure 8, with the Mean of the datasets being 1.00034, with the standard deviations 1.4×10^{-5} and 1.1×10^{-5} for May 2023 and March 2024 respectively. Our expected value R_{XY} derived in [2] is 1.00035. The calculated and expected values agree at 0.001 % level. The small measured variations indicate that the response function ratio changes may not be significant in explaining the observed long-term drift (100 times larger) in the pcal calibration comparison.

Conclusions

Issues encountered by the Kenyon group with populating the influxDB database, limited the data available to six days at the start of the O4 observing run. However, this short stretch of data provided a *playground* for developing the methods reported here and a first look at the variations in the DARM signal response function over the two 0.1 Hz separation of the two Pcal frequencies. The observed relative variation in the response function ratio over these six days was 0.001 %. This indicates that it is not likely that it contributes significantly to the 0.2 % variation observed during the first 35 weeks of the run (see Figure 2). However, we do not have enough data to make a definitive conclusion. Currently, the database issues seem to have been resolved and we are currently populating the influxDB database with more CC_{Derr} data in order to extend our analysis of the behavior of R_{XY} during the entire first 35 weeks of the observing run.

References

[1] Bhattacharjee D, Lecoeuche Y, Karki S *et al* 2020 Fiducial displacements with improved accuracy for the global network of gravitational wave detectors *Class. Quantum Grav.* **38** 015009.

[2] R. Savage, J. Betzweiser, and D. Bhattacharjee. Updating Pcal combined displacement correction factors and evaluating Pcal systematic errors during the O4b observing run -*LIGO technical report* LIGO-T2400108.

[3] Sun L, Goetz E, Kissel J S *et al* 2020 Characterization of systematic error in Advanced LIGO calibration *Class. Quantum Grav.* **37** 225008.

[4] A. D. Viets *et al* 2018 Reconstructing the calibrated strain signal in the Advanced LIGO detectors *Class. Quantum Grav.* **35** 095015.

[5] Grafana Labs. Grafana documentation, 2018.

[6] Aguinis, H., Gottfredson, R. K., amp; Joo, H. (2013). Best-Practice Recommendations for Defining, Identifying, and Handling Outliers. *Organizational Research Methods*, **16**(2), 270-301.

[7] Ford C. 2020. "Understanding empirical cumulative distribution functions."UVA Library StatLab.